ACS OMEGA

Open Access

http://pubs.acs.org/journal/acsodf

Article

Investigation on the Drug Release Efficacy of the Ibuprofen-Loaded ZIF-8/Fe_3O_4 NPs Nanocarrier

Anindita Chakraborty, Rajat Nandi, Diwakar Kumar, and Himadri Acharya*

Cite This: *ACS Omega* 2024, 9, 32418−32428

Read Online

ACCESS | Metrics & More | Article Recommendations | Supporting Information

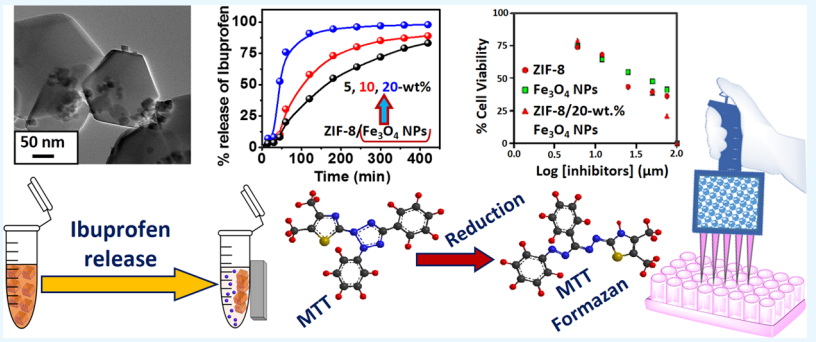

ABSTRACT: In this work, a one-pot multicomponent synthesis of the ibuprofen-loaded Fe_3O_4 nanoparticles-supported zeolitic imidazolate framework-8 (Ibu-ZIF-8/Fe_3O_4 NPs) nanohybrid was carried out. The ZIF-8/Fe_3O_4 NPs nanohybrid was used as a drug carrier for the *in vitro* release of ibuprofen in a PBS solution. The structure and morphology of the synthesized materials were investigated by powder X-ray diffraction (PXRD) analysis, transmission electron microscopy (TEM) analysis, UV−visible absorption studies, FTIR spectroscopy, and thermogravimetric analysis (TGA). The ibuprofen release kinetics was studied by UV−visible spectroscopy. The mechanism of drug delivery was thoroughly investigated and the Higuchi model was found as the best-fitted model for the ibuprofen release study. The 20 wt % Fe_3O_4 NPs-supported ZIF-8 nanohybrid exhibited more than 95% ibuprofen release efficiency in phosphate buffer saline of pH 7.4 within 2 h. The separation ability of the nanohybrid was very good, and it was easily separated by a simple commercial magnet. In order to investigate the cell viability, the cytotoxicity of ZIF-8, Fe_3O_4 NPs, and ZIF-8/20 wt % Fe_3O_4 NPs was investigated using MTT assays against *Leishmania donovani* promastigotes. The ZIF-8/20 wt % Fe_3O_4 NPs nanohybrid carrier exhibited a cell growth inhibition effect with a high correlation coefficient and low probability (p) values. The high release of drug molecules may be due to the more open site of the ZIF-8/Fe_3O_4 NPs nanohybrid. The drug release profile suggests that the nanohybrid can be potentially used as a drug carrier for targeted drug delivery systems.

1. INTRODUCTION

Drug release or drug delivery is the process of releasing pharmaceutically active compounds into the body to obtain the desired therapeutic actions. However, pharmaceutical compounds have a very high molecular weight, or sometimes they are insoluble in aqueous medium. Therefore, to achieve better therapeutic action, the drug materials are required to bind with some carrier materials for the targeted drug delivery process.[1] Two types of carriers generally work in the drug delivery system: one is the organic carrier, which includes polymer materials, micelles, liposomes, and protein nanoparticles, and the other includes porous materials such as zeolites, mesoporous silica, etc.[2−6] The porous materials are advantageous over other organic carriers due to their well-defined porosity and flexibility, which help in greater loading of drug molecules as well as their controlled release.[7,8] Despite various types of mesoporous materials, metal organic frameworks (also called supramolecular solids) are extensively used as drug carriers, as they possess a regular porosity, a large pore volume, flexible pore sizes with high thermal and chemical stability, and organic functionality.[1,9,10] They are constructed by metal atoms or metal clusters, called secondary building units (SBUs), connected with multidentate organic ligands with coordinate bonds.[11] Structurally, metal organic frameworks contain hydrophilic and hydrophobic units, which help to tune their pore sizes and also help the guest molecules to interact with them. Among all of the metal organic frameworks, the MIL series (Materials of Institut Lavoisier) was the first series used in the drug delivery system. In an earlier report, Férey et al. worked on the adsorption, storage, and release of a model

Received: November 16, 2023
Revised: March 12, 2024
Accepted: March 18, 2024
Published: July 19, 2024

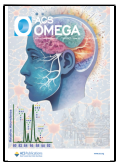

molecule, ibuprofen (an anti-inflammatory drug), with the help of rigid chromium-based MIL-101 and MIL-100 frameworks. The great storage capacities of these MILs persisted for 3−6 days due to their large pore sizes (25−34 Å) as well as large surface areas (3100−5900 m^2/g). Both Cr-based MIL-101 and MIL-100 exhibited the loading of 1.376 and 0.347 g of ibuprofen in their cavities.[12] It is worth mentioning that chromium and heavy metals are very toxic to living systems. Hence, the development of nontoxic, biocompatible drug carriers is a great challenge for the sustainable drug delivery process.[13,14] In this context, zeolitic imidazolate frameworks (ZIFs) are considered as the most nontoxic and biocompatible metal organic frameworks along with high thermal and chemical stability, well-defined pores, and a high specific surface area.[15] Moreover, for drug delivery, the zeolitic imidazolate frameworks are more advantageous over other metal organic frameworks, as they can fabricate pH-responsive drug delivery systems.[16] ZIF-8, the most representative zeolitic imidazolate framework, has a sodalite zeolite-type topology consisting of Zn^{2+} ions as secondary building units and 2-methylimidazole as a linker.[17] Recently, ZIF-8 and its composites with other functional materials have been extensively used in various biomedical applications, especially in the drug delivery process, because of their dissolution in acidic or neutral media.[18−23]

Although metal organic frameworks are studied as potential drug carriers, there are still some drawbacks due to their cytotoxic effect inside living systems. The report suggests that metal organic frameworks including ZIF-8 or other organic or inorganic drug carriers such as polymeric micelles, nonionic lipids and surfactants, mesoporous silica nanoparticles, gold nanoparticles, or iron oxide nanoparticles can be cytotoxic for the *in vivo* drug delivery process when they are accumulated in nontargeted organs.[24−27] The major disadvantage of nanoparticles-based drug carriers such as gold nanoparticles or iron oxide nanoparticles is that sometimes they produce free radicals inside the living systems due to their active surface functional groups.[28] Hence, a targeted drug delivery process coupled with biocompatible surface functional groups of the drug carriers is the only way to address this challenge. With that intention, we have prepared a citrate-stabilized Fe_3O_4 nanoparticles-supported ZIF-8 nanohybrid as a drug carrier for the *in vitro* release of the nonsteroidal, anti-inflammatory, potential drug "ibuprofen". The incorporation of citrate-stabilized Fe_3O_4 nanoparticles into ZIF-8 helps to maintain the biocompatibility of the nanohybrid and leads to the targeted drug delivery process due to the induced magnetic property of the nanohybrid for the incorporation of Fe_3O_4 nanoparticles.

In this work, one-pot multicomponent synthesis was carried out to prepare the ibuprofen-loaded Fe_3O_4 NPs-supported ZIF-8 nanohybrid. The drug release efficiency of the nanohybrid was studied by using a UV−visible spectrophotometer. The control experiment was carried out with pristine ZIF-8. We have thoroughly studied the mechanism of the *in vitro* release of ibuprofen. Finally, the cell viability and the cytotoxicity of ZIF-8, Fe_3O_4 NPs, and the ZIF-8/Fe_3O_4 NPs nanohybrid were investigated using MTT assays against *Leishmania donovani* promastigotes.

2. EXPERIMENTAL SECTION

2.1. Chemicals. Ferric chloride hexahydrate [$FeCl_3·6H_2O$, 99%], ferrous sulfate heptahydrate [$FeSO_4·7H_2O$, 99%], ammonia [28%], trisodium citrate dihydrate [$C_6H_5Na_3O_7·2H_2O$, 99%], zinc nitrate hexahydrate [$Zn(NO_3)_3·6H_2O$, 99%], 2-methylimidazole [$C_4H_6N_2$, 99%], and ibuprofen [$C_{13}H_{18}O_2$, 98%] were purchased from various commercial suppliers such as Sigma-Aldrich, and laboratory grade methanol, NaOH pellets, NaCl, KCl, Na_2HPO_4, KH_2PO_4, HCl (0.1M) from Fisher Scientific Chemical Co., Ltd. All chemicals were used as received without further purification. Deionized water was used in all of the experimental processes.

2.2. Characterization. Powder X-ray diffraction (PXRD) analysis was carried out using a BRUKER-D8 Advance X-ray diffractometer with Cu−K_α radiation at λ = 1.5418 Å passed through a 0.04 rad Soller slit, a 1.0 mm fixed mask with a 1.0° divergence slit, and a 0.2° antiscatter slit. The size and morphology of the Ibu-ZIF-8/Fe_3O_4 NPs nanohybrid were observed with a JEOL JEM-2100 transmission electron microscope operated at 200 kV. The sample preparation was done by drop-casting the ethanolic dispersion of the sample on a 200-mesh-sized carbon-coated copper grid and dried overnight in air before characterization. The UV−visible absorption spectra were recorded with a JASCO V-670 spectrophotometer with a 1 nm data interval in the range of 200−800 nm and in the NIR range. Thermogravimetric analyses of the synthesized materials were performed using a PerkinElmer STA 6000 instrument in the temperature range of 40−830 °C. Fourier transform infrared (FTIR) spectra were recorded through a PerkinElmer L 120−000A spectrometer (λ_{max} in cm^{-1}) using the KBr disc method in the range of 4000−400 cm^{-1}, with the scan speed of 200 nm min^{-1}.

2.3. Synthesis of Citrate-Stabilized Fe_3O_4 NPs. Citrate-stabilized Fe_3O_4 nanoparticles were prepared by a coprecipitation method. In a typical synthesis, a 50 mL aqueous solution containing a stoichiometric amount of $FeCl_3·6H_2O$ (2 g, 0.007 mol) and $FeSO_4·7H_2O$ (3.8 g, 0.013 mol) was taken. Ammonia solution (28%, 4 mL) was added dropwise to the above mixture, and the mixture was stirred mechanically at 90 °C for 15 min. Next, trisodium citrate dihydrate ($C_6H_5Na_3O_7·2H_2O$) (4.5 g, 0.015 mol) was added to the above reaction mixture and stirred for another 30 min. The resulting dark brown precipitate was collected by the magnetic separation process and washed several times with a water/methanol mixture and dried at 75 °C in a hot air oven.

2.4. One-Pot Synthesis of the Ibuprofen-Loaded Fe_3O_4 Nanoparticles-Supported Zeolitic Imidazolate Framework-8 (Ibu-ZIF-8/Fe_3O_4 NPs) Nanohybrid. In a typical synthesis, an aqueous dispersion of citrate-stabilized Fe_3O_4 NPs (0.150 g) was prepared in 20 mL of deionized water. Subsequently, 30 mL of solution containing $Zn(NO_3)_2·6H_2O$ (1.5 g, 0.005 mol) followed by 20 mL of solution of 2-methylimidazole (3.3 g, 0.040 mol) was added to the above reaction mixture. After a few minutes, ibuprofen (0.100 g) was added, and the reaction mixture was stirred vigorously for 2 h at room temperature. The resulting brown precipitate was collected with magnetic separation, washed with methanol several times, and dried in a vacuum desiccator. In this process, the product obtained was 3 g, where Fe_3O_4 NPs and ibuprofen contents were, respectively, 5 and 3.3 wt %. The similar procedure was adopted for the synthesis of 3.3 wt % Ibu-ZIF-8/Fe_3O_4 NPs nanohybrids (where Fe_3O_4 NPs contents were 10 and 20 wt %) and Ibu-ZIF-8/20 wt % Fe_3O_4 NPs nanohybrids (where ibuprofen contents were 1, 2, and 5 wt %). The loss of ibuprofen during the washing process was completely ruled out, as the UV−visible absorption spectrum

https://doi.org/10.1021/acsomega.3c09135
ACS Omega 2024, 9, 32418−32428

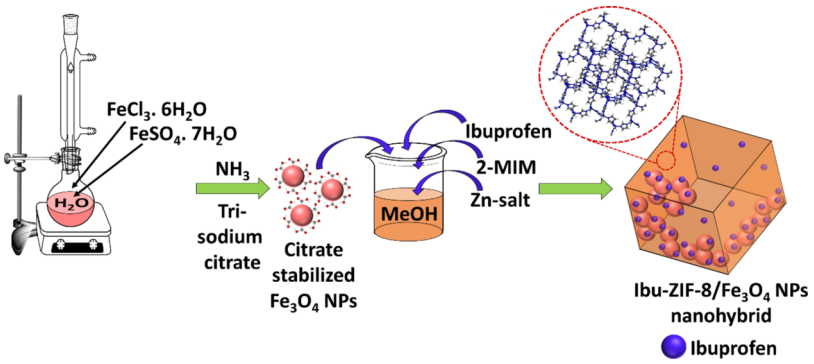

Figure 1. Schematic representation of the formation of the ibuprofen-loaded Fe_3O_4 NPs-supported ZIF-8 nanohybrid.

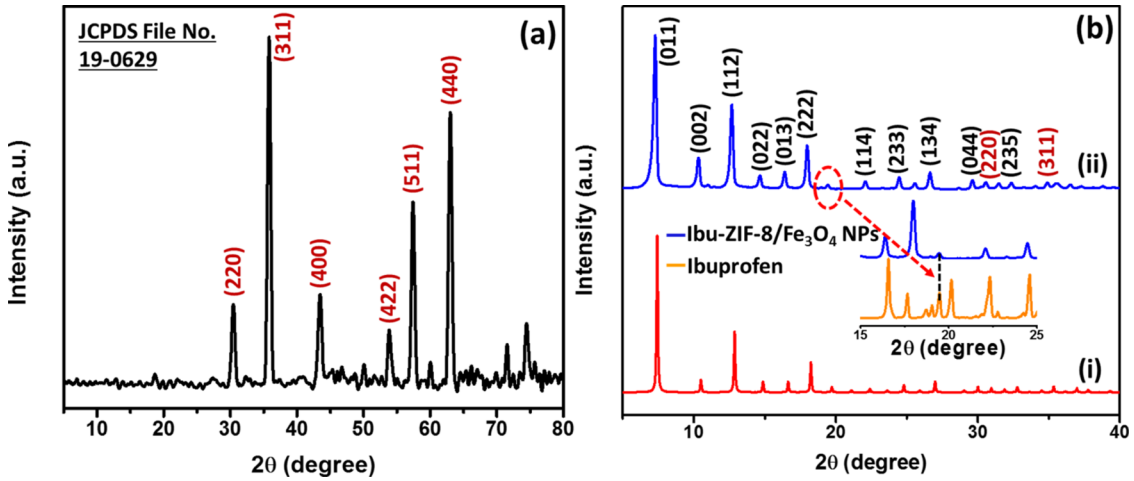

Figure 2. (a) PXRD patterns of synthesized Fe_3O_4 NPs and (b) (i) the simulated XRD pattern of ZIF-8 and (ii) the PXRD pattern of the 3.3 wt % Ibu-ZIF-8/5 wt % Fe_3O_4 NPs nanohybrid. The planes due to ZIF-8 and Fe_3O_4 NPs are shown in "black" and "red" colors, respectively. The inset image in panel (b) shows the PXRD patterns of ibuprofen and the synthesized nanohybrid from the 2θ range of 15 to 25°.

of the supernatant solution did not show any noticeable absorption peak for ibuprofen. Therefore, it could be assumed that the total amount of ibuprofen taken for one-pot multicomponent synthesis was entirely loaded into the nanohybrid.

2.5. Ibuprofen Release Study. The ibuprofen release study was carried out in a 50 mL glass flask, containing the Ibu-ZIF-8/Fe_3O_4 NPs nanohybrid (20 mg) in phosphate buffer solution at pH 7.4 (30 mL). First, the drug-loaded matrix was dispersed in the PBS solution with vigorous stirring at 37 °C. After a particular time interval, aliquot portions of the PBS solution were withdrawn and the drug-loaded matrix was removed by the magnetic separation process. The amount of ibuprofen released in the PBS solution was measured by UV−visible spectroscopy. The proficiency of the matrix was evaluated over a wide range of matrix concentrations in the PBS solution and also with the varying composition of Fe_3O_4 NPs and ibuprofen in the nanohybrid, under identical conditions. ZIF-8 was taken as a control in the drug release study. The fraction of ibuprofen release in the PBS solution after a particular time (f_t) is given by

$$f_t(\%) = \frac{M_t}{M_0} \times 100 \quad (1)$$

where M_t is the amount of ibuprofen released from the matrix at a particular time and M_0 is the total amount of ibuprofen initially present in the matrix.

However, the ibuprofen release mechanism can be ascertained by fitting the drug release data into the kinetic models as follows:

Zero-order model:

$$f_t = k_0 t \quad (2)$$

First-order model:

$$\ln(1 - f_t) = k_1 t \quad (3)$$

Higuchi model:

$$f_t = k_H t^{1/2} \quad (4)$$

Korsmeyer−Peppas model:

$$f_t = k_P t^n \quad (5)$$

where f_t is the fraction of ibuprofen release at time t (min). k_0, k_1, k_H, and k_P are the rate constants of zero-order, first-order, Higuchi, and Korsmeyer−Peppas kinetic models, respectively, and n is the drug release exponent.[29,30]

2.6. Cytotoxicity Assay. *In vitro* inhibitory effects of developed compounds (ZIF-8, Fe_3O_4 NPs, and ZIF-8/20 wt % Fe_3O_4 NPs) against *Leishmania donovani* promastigotes were assessed using the MTT test.[31] Promastigotes were grown in T25 tissue culture flasks at 25 °C. These cells were planted into individual wells of 96-well plates with 100 μL of M199 medium at a density of 2×10^6 cells/well and incubated

https://doi.org/10.1021/acsomega.3c09135
ACS Omega 2024, 9, 32418−32428

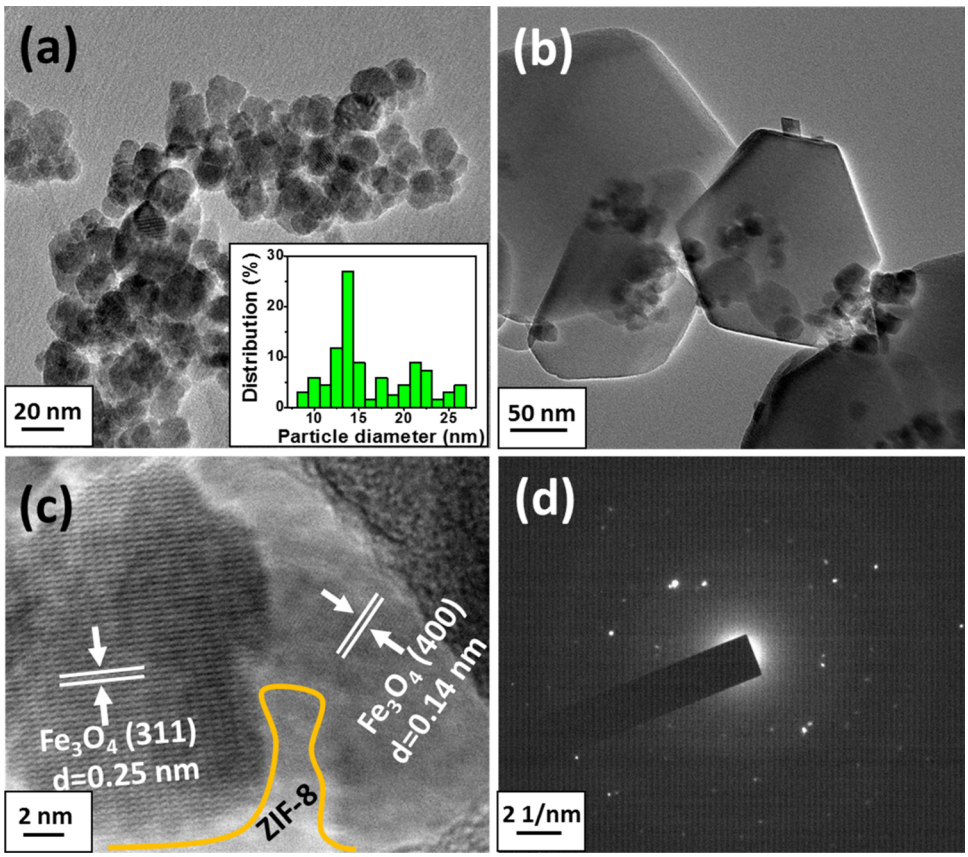

Figure 3. (a) Representative TEM image of Fe_3O_4 NPs (the inset image shows the particle size distribution of Fe_3O_4 NPs), (b) TEM image of the 3.3 wt % Ibu-ZIF-8/5 wt % Fe_3O_4 NPs nanohybrid, (c) HRTEM image of the 3.3 wt % Ibu-ZIF-8/5 wt % Fe_3O_4 NPs nanohybrid showing (311) and (400) planes of Fe_3O_4 NPs, and (d) SAED pattern of the 3.3 wt % Ibu-ZIF-8/5 wt % Fe_3O_4 NPs nanohybrid.

overnight. Following an overnight incubation, the cells were exposed to different doses of the chemicals, including ZIF-8, Fe_3O_4 NPs, and the ZIF-8/20 wt % Fe_3O_4 NPs nanohybrid as well as an Amphotericin B positive control. Simultaneously, untreated cells were employed as a negative control. These preparations were incubated overnight, and each experiment was repeated three times. After that, the cells were collected, and the culture medium was removed. The cells were cultured in the dark for 4 h at 25 °C after being treated with the MTT reagent (5 mg/mL). The MTT reagent was carefully aspirated after incubation, and a 100 μL/well MTT solubilizer was applied to dissolve the formazan crystals. The reduction in MTT was determined by measuring the absorbance of the microtiter plate at 570 nm with a microtiter plate reader.

3. RESULTS AND DISCUSSION

The Ibu-ZIF-8/Fe_3O_4 NPs nanohybrid was prepared by one-pot multicomponent synthesis. The schematic representation of the formation of the nanohybrid is shown in Figure 1. Initially, Fe_3O_4 nanoparticles were prepared by the chemical coprecipitation method in an aqueous medium and were subsequently used as supporting materials for the in situ nucleation and growth of ZIF-8 crystals on their surfaces.

3.1. Powder X-ray Diffraction (PXRD) Analysis. In order to investigate the crystal structure of synthesized materials, powder X-ray diffraction analysis was carried out, and the results are shown in Figure 2. Figure 2a represents the PXRD profile of Fe_3O_4 nanoparticles, where the well-defined peaks at 2θ values of 30.4, 35.7, 43.4, 53.8, 57.3, and 63.0° represent the highly crystalline, fcc lattice structure of magnetite nanoparticles [JCPDS file no. 19-0629].[32] The average crystallite size of 14.4 nm is obtained from Debye–Scherrer's equation of paramagnetic Fe_3O_4 nanoparticles.[33] The diffraction pattern of the Ibu-ZIF-8/Fe_3O_4 NPs nanohybrid, as shown in Figure 2b(ii), shows the combination of diffraction peaks of ZIF-8 and Fe_3O_4 NPs. The peaks present in the 2θ range of 5–30° are the typical diffraction peaks of ZIF-8, which are consistent with the simulated XRD pattern of the ZIF-8 single crystal, as shown in Figure 2b(i). The peak positions at 7.2, 10.3, 12.6, 14.6, 16.4, 17.9, 22.0, 24.4, 26.6, 29.6, and 32.3° are indexed as the (011), (002), (112), (022), (013), (222), (114), (233), (134), (044), and (235) crystal planes of ZIF-8, respectively.[17] Moreover, the noticeable weak peaks observed in the PXRD pattern of the nanohybrid at 30.5, 34.9, 56.7, and 62.8° 2θ values are indexed as the (220), (311), (511), and (440) planes of Fe_3O_4 NPs, respectively [Figure S1]. Furthermore, a very weak reflection observed at the 2θ position of 19.5° is originated due to the presence of ibuprofen [inset, Figure 2b].

3.2. Transmission Electron Microscopy (TEM) Analysis. The size and morphology of the synthesized materials were investigated by transmission electron microscopy analysis. The TEM image of Fe_3O_4 NPs shown in Figure 3a indicates the uniform distribution of the nanoparticles with an average dimension of ~15 nm, which is in strong agreement with the crystallite size obtained from PXRD analysis. The uniform distribution reveals the good dispersion of Fe_3O_4 NPs in the solution. From TEM analysis, it is clear that the majority of the

https://doi.org/10.1021/acsomega.3c09135
ACS Omega 2024, 9, 32418–32428

Fe_3O_4 NPs are crystalline and cubic in shape. However, typical high-magnification and high-resolution TEM images of the Ibu-ZIF-8/Fe_3O_4 NPs nanohybrid are shown in Figure 3b,c. The apparent color variations observed from these images suggest the heterostructure formation. The high-magnification TEM image clearly shows the nanoparticles (appearing as the darker contrast), which are very orderly incorporated into the ZIF-8 cubes (appearing as the lighter contrast) of size ~150 nm. Furthermore, a clear grain boundary between Fe_3O_4 NPs and ZIF-8 crystals can be distinguished from the HRTEM image. However, the interplanar spacings of 0.25 and 0.14 nm are calculated for darker regions, which correspond to the typical (311) and (400) planes of Fe_3O_4 NPs, respectively. Moreover, the SAED pattern shown in Figure 3d further confirms the polycrystalline nature of the nanohybrid.

3.3. Fourier Transform Infrared (FTIR) Spectral Analysis. Figure 4 represents the FTIR spectra of citrate-stabilized Fe_3O_4 NPs and the ibuprofen-loaded ZIF-8/Fe_3O_4 NPs nanohybrid. Citrate-stabilized Fe_3O_4 NPs shown in Figure 4(i) exhibit a strong band around 1623 cm^{-1}, which appears to be due to the C═O stretching vibration of citrate ions. This C═O stretching vibration is 41 cm^{-1} shifted toward a lower wavenumber value in comparison to pure citrate ions [Figure S2a], which may be due to the interaction between the Fe ions and C═O groups of trisodium citrate. However, two additional vibrational bands, observed around 1408 and 1262 cm^{-1}, are assigned to the symmetric COO^- and C−O stretching vibrations of carboxylate groups, respectively. The absorption bands observed between 630−560 cm^{-1} are associated with the Fe−O stretching vibrations of Fe_3O_4 nanoparticles.[34]

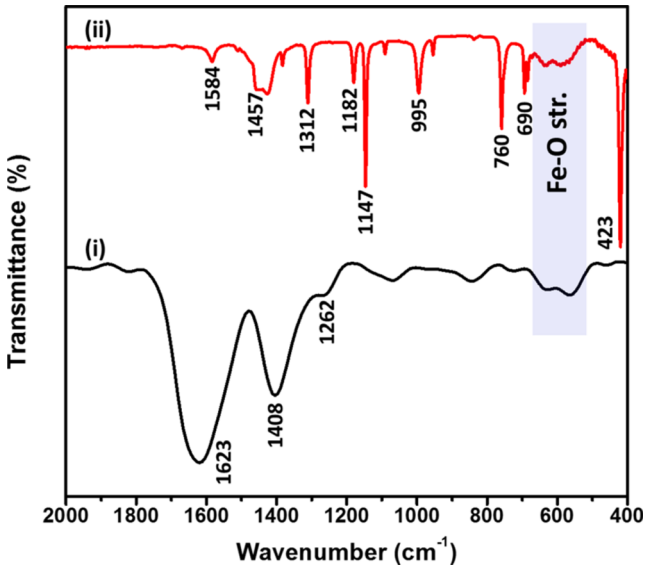

Figure 4. FTIR spectra of (i) Fe_3O_4 NPs and (ii) the 3.3 wt % Ibu-ZIF-8/5 wt % Fe_3O_4 NPs nanohybrid.

The FTIR spectrum of the Ibu-ZIF-8/Fe_3O_4 NPs nanohybrid shown in Figure 4(ii) represents the absorption bands around 1584 and 1457 cm^{-1}, which appear due to the C═N and C−N stretching vibrations of imidazole, respectively.[17] The sharp bands recorded between 1312 to 995 cm^{-1} are associated with the in-plane bending vibrations of the imidazole ring. Two additional sharp bands observed at 760 and 690 cm^{-1} can be attributed to the aromatic sp^2 C−H bending vibrations of the linker moiety.[35] The presence of moderately strong absorption bands between 630−560 cm^{-1} is due to the characteristic Fe−O stretching vibrations of Fe_3O_4 NPs.[34] The typical Zn−N stretching vibration appears at 423 cm^{-1}. Two vibrational bands observed around 3216 and 3136 cm^{-1} are attributed to the N−H and aromatic C−H stretching vibrations of imidazole, respectively. Furthermore, the bands present in the region of 2966−2885 cm^{-1} are associated with the aliphatic C−H stretching vibrations, which appear due to the presence of ibuprofen [Figure S2b].[36] The FTIR spectra of ZIF-8, Ibu-ZIF-8, and ZIF-8/Fe_3O_4 NPs are shown in Figure S2c. All three compounds show the characteristic bands for the C═N and C−N stretching vibrations of the imidazole ring (around 1588 and 1435 cm^{-1}), the in-plane bending vibrations of the imidazole ring (between 1311 to 996 cm^{-1}), the aromatic sp^2 C−H bending vibrations (around 756 and 689 cm^{-1}), and the Zn−N stretching vibration (around 423 cm^{-1}) for ZIF-8 structures. Additionally, Ibu-ZIF-8 exhibits bands between 2962 and 2890 cm^{-1}, which are associated with the aliphatic C−H stretching vibrations of ibuprofen molecules.

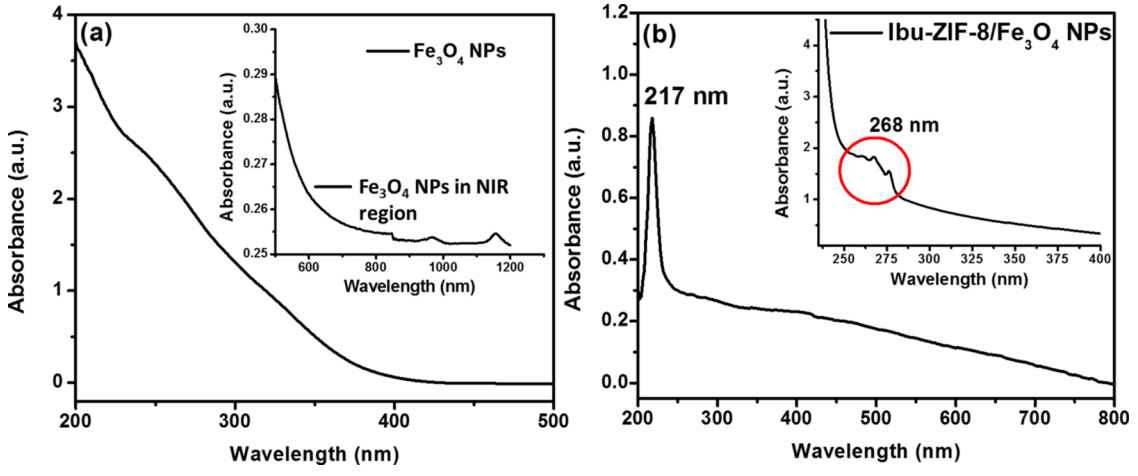

Figure 5. UV−visible absorption spectra of (a) Fe_3O_4 NPs (the inset image shows the absorption spectrum of Fe_3O_4 NPs in the NIR region) and (b) the 3.3 wt % Ibu-ZIF-8/5 wt % Fe_3O_4 NPs nanohybrid (the inset shows the peak for ibuprofen in the 3.3 wt % Ibu-ZIF-8/5 wt % Fe_3O_4 NPs nanohybrid).

https://doi.org/10.1021/acsomega.3c09135
ACS Omega 2024, 9, 32418−32428

Furthermore, the ZIF-8/Fe_3O_4 NPs nanohybrid exhibits characteristic Fe−O stretching vibration between 634 and 580 cm^{-1}. A shift of the aliphatic C−H stretching vibrations and aromatic sp^2 C−H bending vibrations of drug molecules in the nanohybrids (Figure S2b,c) to the high frequency compared to pure ibuprofen or ZIF-8 indicates the interactions of drug molecules with the nanocarrier.

3.4. UV−Visible Analysis. The UV−visible absorption spectra of citrate-stabilized Fe_3O_4 NPs and the Ibu-ZIF-8/Fe_3O_4 NPs nanohybrid are shown in Figure 5. The absorption spectrum of Fe_3O_4 nanoparticles shown in Figure 5a exhibits a continuous absorption band covering a broad range of absorption profiles from the UV to the NIR regions. The broad absorption can be associated with the intervalence charge transfer (IVCT) transition between ferrous and ferric ions.[37,38] Figure 5b represents the UV−visible absorption spectrum of the Ibu-ZIF-8/Fe_3O_4 NPs nanohybrid, which exhibits apparent broadening in the absorptivity in the visible region when compared with pristine ZIF-8 [Figure S3a]. Similarly, Ibu-ZIF-8 and the ZIF-8/Fe_3O_4 NPs nanohybrid also exhibit broadening in the absorption spectra, as compared with pristine ZIF-8 [Figure S3a]. The broadening in the absorption spectra is associated with the predominant surface defects due to the incorporation of ibuprofen molecules and Fe_3O_4 NPs.[39] Moreover, a small hump is observed at 268 nm in the UV−visible spectrum of the Ibu-ZIF-8/Fe_3O_4 NPs nanohybrid, which confirms the successful loading of ibuprofen molecules into the nanohybrid [Figure S3b].[40] The UV−visible spectrum of Ibu-ZIF-8 also exhibits a small hump at around 265 nm due to ibuprofen loading. However, the peaks for ibuprofen in the Ibu-ZIF-8/Fe_3O_4 NPs nanohybrid and Ibu-ZIF-8 exhibit a 4 and a 1 nm red shift, respectively, in comparison to free ibuprofen molecules, which further supports the strong interaction between ibuprofen and ZIF-8/Fe_3O_4 NPs or ZIF-8.

3.5. Thermogravimetric Analysis. The thermogravimetric analysis (TGA) of the as-synthesized materials is shown in Figure 6. The TGA curve of citrate-stabilized Fe_3O_4 nanoparticles shows an initial weight loss of 2 wt % in the temperature range of 35 to 195 °C, which is due to the loss of guest molecules adsorbed on the surface of nanoparticles. The second weight loss (3 wt %) occurs from 195−320 °C and is associated with the removal of the nanoparticle's capping agent (trisodium citrate). A long plateau above 325 °C is observed in the TGA profile of Fe_3O_4 NPs with only a loss of 2 wt %, suggesting the high thermal stability of the nanoparticles.[41] TGA curves of ZIF-8, Ibu-ZIF-8, and the ZIF-8/Fe_3O_4 NPs nanohybrid are provided in the Supporting Information [Figure S4a]. ZIF-8 shows a loss of 2.5 wt % up to 180 °C for the loss of some solvent or guest molecules. In between 180−500 °C, the 14 wt % loss occurs due to adsorbed linkers and beyond 500 °C, the framework starts decomposing. The TGA profile of Ibu-ZIF-8 shows similarity with pristine ZIF-8. Ibu-ZIF-8 exhibits a loss of 3 wt % up to 240 °C for the removal of the solvent or other guest species along with ibuprofen. From 240−560 °C, the decomposition of 13 wt % occurs due to the adsorbed linker and beyond 560 °C, the framework starts decomposing. The TGA profile of the ZIF-8/Fe_3O_4 NPs nanohybrid exhibits much increase in thermal stability compared to ZIF-8. The compound shows a loss of 25 wt % in the temperature between 140−635 °C for the decomposition of solvent molecules/guest species and adsorbed linker molecules, and beyond 635 °C, the framework structure of the ZIF-8/Fe_3O_4 NPs nanohybrid starts disintegrating. The TGA curve of the ibuprofen-loaded Fe_3O_4 nanoparticles-supported ZIF-8 nanohybrid also exhibits much thermal stability when compared with that of pristine ZIF-8. The Ibu-ZIF-8/Fe_3O_4 NPs nanohybrid shows a three-stage decomposition process with a first weight loss of 3% above 120 °C and continues up to 265 °C, which is associated with the decomposition of ibuprofen along with some other guest species occluded into the framework structure [Figure S4b]. The material exhibits a second-stage weight loss of 27% in the temperature zone of 265−655 °C, which is attributed to the evacuation of some adsorbed linker molecules. In the third stage of the weight loss process (beyond 610 °C), the ZIF-8 framework structure starts disintegrating and completely collapses into solid oxide materials.[17]

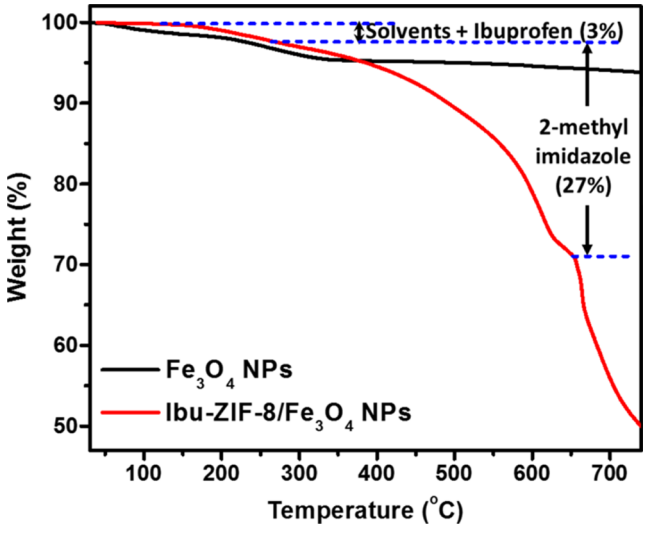

Figure 6. TGA curves of Fe_3O_4 NPs and the 3.3 wt % Ibu-ZIF-8/5 wt % Fe_3O_4 NPs nanohybrid.

3.6. Ibuprofen Release Study. The *in vitro* release of ibuprofen in the PBS solution in the presence of the ZIF-8/Fe_3O_4 NPs nanohybrid is elaborated in Figure 7. Figure 7a represents the time-dependent UV−visible absorption spectra of ibuprofen in the PBS solution of pH 7.4, released from the ZIF-8/20 wt % Fe_3O_4 NPs nanohybrid. The spectra show a gradual increase in the absorption intensity at 273 nm with the release time, indicating the increase in the ibuprofen concentration in the PBS solution. The drug release efficiency of the nanohybrid with the release time is shown in Figure 7b. It is observed that the ibuprofen release efficiency is 95% in the presence of the ZIF-8/20 wt % Fe_3O_4 NPs nanohybrid in 180 min, which is much higher compared to the drug release efficiencies of 5 and 10 wt % Fe_3O_4 NPs-supported ZIF-8 nanohybrids (63 and 73%, respectively). The control experiment was screened with ZIF-8 under similar experimental conditions that took 3 days to release 92% ibuprofen into the PBS solution [Figure S5]. The ZIF-8/Fe_3O_4 NPs nanohybrid also exhibits a much higher drug release efficiency in comparison to other reported carrier materials. The comparative study is summarized in Table 1.[42−45] The enhanced ibuprofen release efficiency of the Fe_3O_4 NPs-supported ZIF-8 nanohybrid can be explained with the specific surface area. The specific surface areas of pristine ZIF-8 and ZIF-8 nanohybrids with 5, 10, and 20 wt % Fe_3O_4 NPs were calculated using the methylene blue adsorption method, which were obtained as

https://doi.org/10.1021/acsomega.3c09135
ACS Omega 2024, 9, 32418−32428

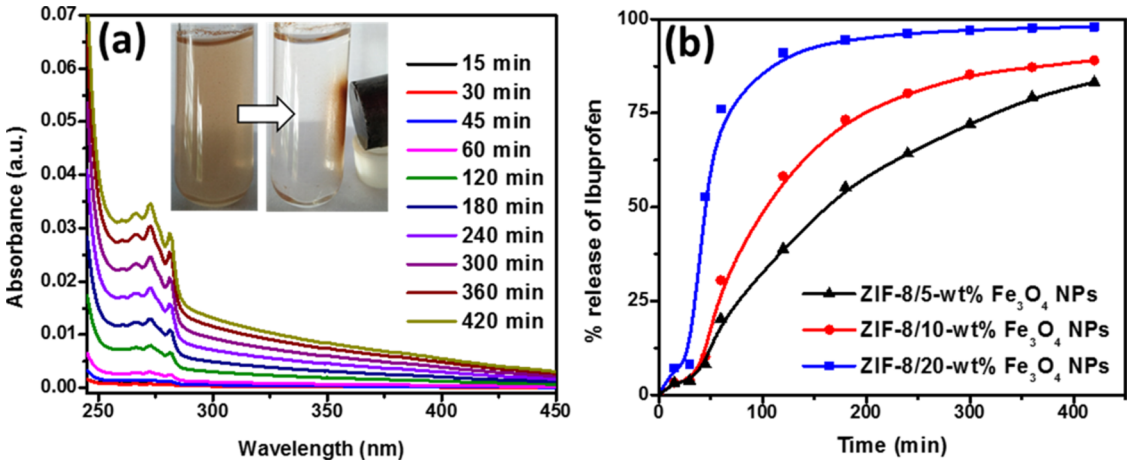

Figure 7. (a) Time-dependent UV−visible absorption spectra recorded during the ibuprofen release study [experimental condition: the 3.3 wt % ibuprofen-loaded ZIF-8/20 wt % Fe_3O_4 NPs nanohybrid (20 mg), the PBS solution of pH 7.4 (30 mL) at 37 °C] (the inset of panel (a) shows the postrelease magnetic separation of the drug molecules from the nanohybrid with a simple commercially available magnet). (b) Plot of drug release efficiencies over the release time in the presence of different matrices [experimental condition: the 3.3 wt % ibuprofen-loaded ZIF-8/Fe_3O_4 NPs nanohybrid (20 mg), the PBS solution of pH 7.4 (30 mL) at 37 °C].

Table 1. Comparison of the *In Vitro* Release of Ibuprofen Facilitated by ZIF-8/Fe_3O_4 NPs Nanohybrids with Literature

entry	carrier used	drug used	drug release medium	time required	percent release	refs
1	Zn_3BTC_2	ibuprofen	PBS	24 h	29	42
2	Ti-based MOF	ibuprofen	PBS	24 h	95	43
3	MIL-100(Fe)	ibuprofen	SBF	3 days	∼100	44
4	MIL-101(Fe)	ibuprofen	SBF	6 days	∼100	44
5	$\{Zn_2(1,4\text{-bdc})_2(dabco)\}_n$	ibuprofen	SBF	12 days	80	45
6	ZIF-8/5 wt % Fe_3O_4 NPs nanohybrid	ibuprofen	PBS	420 min	83	this work
7	ZIF-8/10 wt % Fe_3O_4 NPs nanohybrid	ibuprofen	PBS	420 min	89	this work
8	ZIF-8/20 wt % Fe_3O_4 NPs nanohybrid	ibuprofen	PBS	420 min	97	this work

31.82, 71.52, 77.24, and 82.04 m^2/g, respectively.[34] It is worth mentioning that as the nanoparticles' content in the nanohybrid increases from 5 to 20 wt %, the specific surface area also increases. Therefore, most of the ibuprofen molecules have a tendency to attach to the surface of the nanohybrid rather than entering the hydrophobic pores of ZIF-8 moieties, which leads to the enhanced release rate of drug molecules.[46] However, considering the highest ibuprofen release efficiency, the 20 wt % Fe_3O_4 NPs-supported ZIF-8 nanohybrid was chosen for other parametric studies.

The effect of ibuprofen dosage on the release study was optimized by performing the same set of experiments in the presence of the 3.3 wt % ibuprofen-loaded ZIF-8/20 wt % Fe_3O_4 NPs nanohybrid at 37 °C, where the drug-loaded matrix concentration was varied from 5−20 mg. The corresponding plot of the release efficiency is shown in the Supporting Information [Figure S6]. It is also observed that the drug release efficiency increases significantly with Fe_3O_4 NPs and reaches a plateau faster. It is anticipated that the drug release performance is triggered by the diffusion process. As the concentration of ibuprofen is much higher in the nanohybrid compared to the PBS solution, the ibuprofen molecules move rapidly toward the PBS solution to attain an equilibrium concentration throughout the medium.[47] Therefore, an enhancement of the drug release efficiency is observed with an increase in the drug-loaded matrix concentration.

The drug-loading capacity of ZIF-8 and the ZIF-8/20 wt % Fe_3O_4 NPs nanohybrid was evaluated by varying drug concentrations as control experiments. The loading capacity of ibuprofen in ZIF-8 and the ZIF-8/Fe_3O_4 NPs nanohybrid was examined to reach 20 and 25 wt %, respectively, without any ibuprofen trace in the supernatant solution. However, excess loading was avoided for the release study because it is believed that high loading may lead to the side crystalline formation of drugs and accumulation on the external surface of carrier molecules as a protective layer. As a result, the drug molecules release poorly in a PBS medium.[48] We have compared the drug release efficacy up to 5 wt % ibuprofen-loaded nanohybrids. It is observed that the drug release efficiency is highest for the 3.3 wt % ibuprofen-loaded ZIF-8/20 wt % Fe_3O_4 NPs nanohybrid, compared to other nanohybrids in 420 min [Figure S7].

The mechanism of ibuprofen release kinetics can be interpreted by correlating the drug release profile with various kinetic models described in eqs 2−5. Among the four models, the drug release data fits well with the Higuchi model, which reveals that the *in vitro* release of ibuprofen in the PBS solution of pH 7.4 follows a diffusion process.[49] However, the value of "*n*" determined from the Korsmeyer−Peppas model can further confirm the diffusion process. The Fickian diffusion pathway can be followed when $n < 0.43$ and $n > 0.85$ refer to the swelling or erosion of the matrix and $0.43 < n < 0.85$ describes the non-Fickian diffusion model.[50] The corresponding plots of different kinetic models are listed in Figure 8. The list of model parameters for all four models is given in Table S1.

3.7. *In Vitro* Cytotoxicity by MTT Assay. MTT assay was used to determine the biological activity of the chemicals

https://doi.org/10.1021/acsomega.3c09135
ACS Omega 2024, 9, 32418−32428

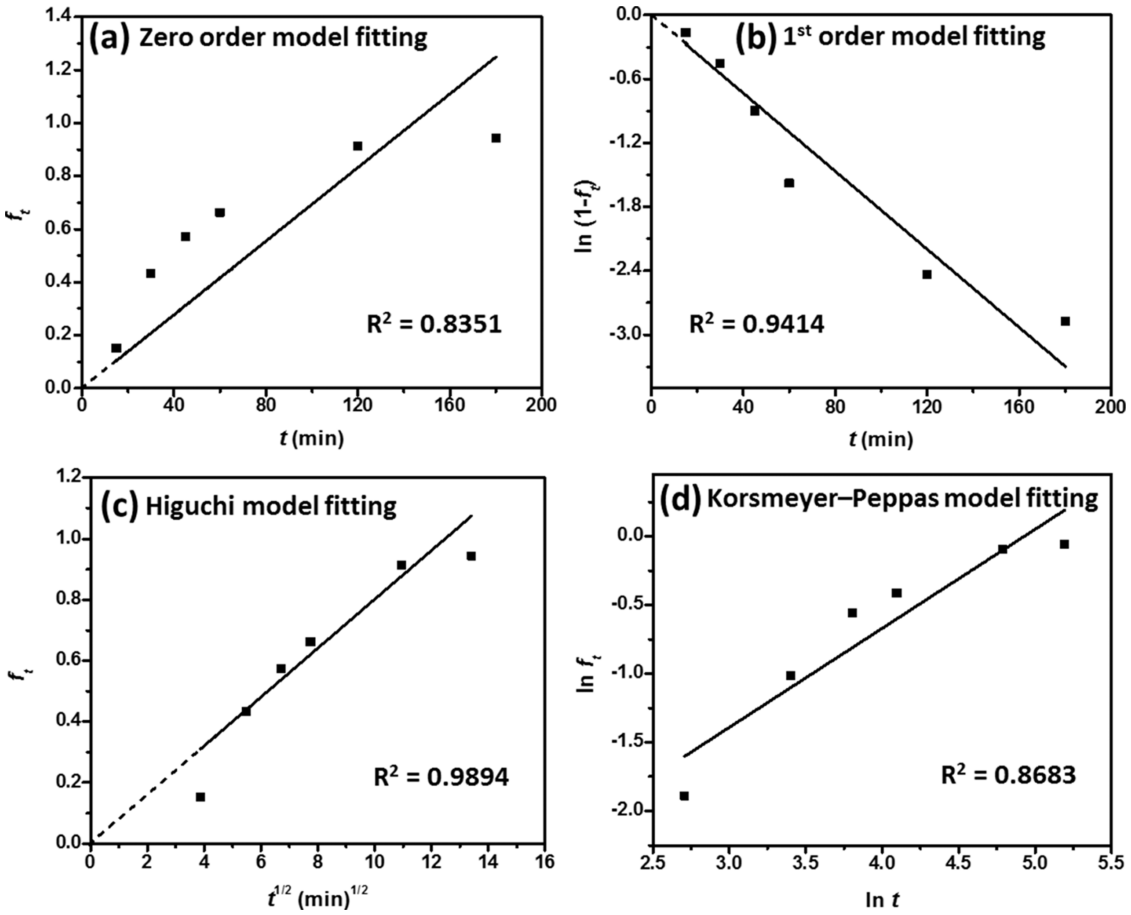

Figure 8. Release kinetics of ibuprofen from the 3.3 wt % Ibu-ZIF-8/20 wt % Fe_3O_4 NPs nanohybrid: (a) zero-order model, (b) first-order model, (c) Higuchi model, and (d) Korsmeyer–Peppas model.

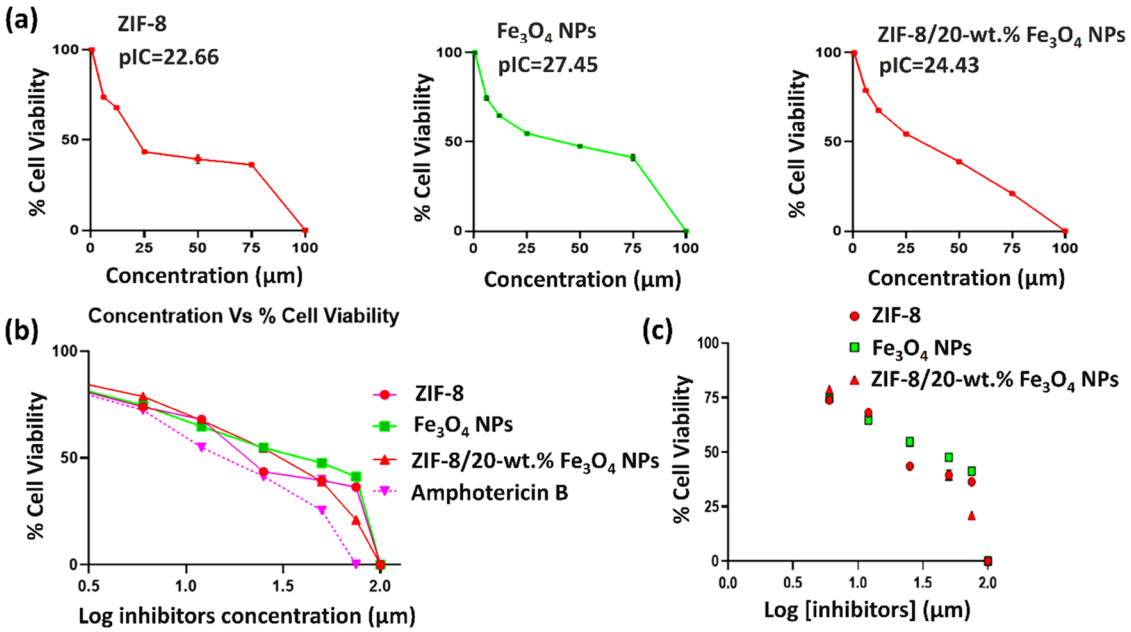

Figure 9. (a) Graph of the MTT experiment of synthesized compounds exhibiting dose–response inhibition in terms of concentration and IC_{50} values. (b) Cell viability percentage graph of ZIF-8, Fe_3O_4 NPs, the ZIF-8/20 wt % Fe_3O_4 NPs nanohybrid, and Amphotericin B. (c) Linear correlation analysis plot of ZIF-8, Fe_3O_4 NPs, and the ZIF-8/20 wt % Fe_3O_4 NPs nanohybrid with *p*-values of 0.0031, 0.0023, and 0.0002, respectively.

produced against *Leishmania donovani* promastigotes and their effectiveness as potential antiparasitic drugs. As specified in the following equation, the results are reported as a percentage of cell viability and are shown in Figure 9.

https://doi.org/10.1021/acsomega.3c09135
ACS Omega 2024, 9, 32418−32428

Table 2. IC_{50} Value and Percentage Cell Viability against Various Concentrations

compounds	6 μM	12 μM	25 μM	50 μM	75 μM	IC_{50} (μM)
ZIF-8	72.72 ± 0.32	68.62 ± 0.12	51.49 ± 0.45	48.63 ± 1.6	46.46 ± 0.77	22.66
Fe_3O_4 NPs	73.24 ± 0.88	66.30 ± 0.64	59.34 ± 0.61	54.34 ± 0.52	49.88 ± 1.2	27.45
ZIF-8/20 wt % Fe_3O_4 NPs nanohybrid	76.12 ± 0.57	68.53 ± 0.30	59.19 ± 0.12	48.24 ± 0.06	35.61 ± 0.26	24.43
Amphotericin B	71.66 ± 0.22	59.49 ± 0.25	49.99 ± 0.96	38.77 ± 0.40	21.08 ± 0.15	14.87

$$\%\ \text{cell viability} = \frac{\text{mean OD of test samples}}{\text{mean OD of control}} \times 100$$

To thoroughly validate this finding, we measured the compound's inhibitory effectiveness throughout a concentration gradient from 6 to 75 μM/mL, as shown in Table 2. Significantly, there was a clear association between an increasing concentration and a corresponding reduction in the viability of *L. donovani*, indicating that the compounds had a robust dose-dependent response. The IC_{50} values for the synthesized compounds, ZIF-8, Fe_3O_4 NPs, and the ZIF-8/20 wt % Fe_3O_4 NPs nanohybrid were 22.66, 27.45, and 24.43 μM, respectively, as shown in Figure 9a,b. Notably, compared with the positive control compound, Amphotericin B, with an IC_{50} of 14.87 μM, these synthesized compounds demonstrated substantial inhibitory activity. This compelling data underscores the potential for further structural refinement of these scaffolds as promising candidates for antileishmanial therapeutics.

Moreover, a meticulous analysis was undertaken, encompassing the linear regression of the compounds, yielding noteworthy correlation coefficients of 0.85, 0.86, and 0.94, respectively. These coefficients signify an exceptionally robust alignment of experimental outcomes, underpinned by significantly low *p*-values of 0.0031, 0.0023, and 0.0002, as depicted in Figure 9c. A rigorous negative control experiment was meticulously executed to assess the potential cytotoxicity stemming from the synthesized compounds. Within this control group, cells were intentionally left unexposed to the compounds, resulting in a cell viability rate of 99.27 ± 1.51%, confirming the efficacy of the synthesized compounds.

4. CONCLUSIONS

In this work, one-pot multicomponent synthesis was successfully carried out to prepare ibuprofen-loaded Fe_3O_4 NPs supported ZIF-8 nanohybrid. The formation of the nanohybrid was examined by PXRD, TEM, FTIR, UV−visible, and TG analyses. The high crystallinity of the nanohybrid is revealed from PXRD data. TEM analysis suggests the formation of cubic-shaped Fe_3O_4 NPs with an average dimension of ∼15 nm. The nanoparticles are well distributed inside the ZIF-8 structure, as reflected by TEM images of the nanohybrid. The potential application of the nanohybrid was explored through the *in vitro* release of the nonsteroidal, anti-inflammatory drug ibuprofen in a PBS solution of pH 7.4. The ZIF-8/20 wt % Fe_3O_4 NPs nanohybrid possesses the highest ibuprofen release efficiency of 95% in 180 min. The release kinetics is significantly enhanced with an increase in nanohybrid concentration and ibuprofen loading in the nanohybrid. The mechanism of drug release kinetics follows the Higuchi model (R^2 = 0.9894) with non-Fickian diffusion. MTT assay on *L. donovani* indicates a low cytotoxicity of the ZIF-8/20 wt % Fe_3O_4 NPs nanohybrid. The cell viability rate of 99.27% ± 1.51% confirms the efficacy of the synthesized compound. All of the consequences can further support the nanohybrid's ability as a potential drug carrier in the field of medicinal/pharmaceutical chemistry.

■ ASSOCIATED CONTENT

Supporting Information

The Supporting Information is available free of charge at https://pubs.acs.org/doi/10.1021/acsomega.3c09135.

PXRD pattern of the Ibu-ZIF-8/Fe_3O_4 NPs nanohybrid in high angle (Figure S1); FTIR spectra (Figure S2), UV spectra (Figure S3), and TGA curves (Figure S4) of some control experiments; ibuprofen release efficiency of ZIF-8 (Figure S5); ibuprofen release efficiency with the ZIF-8/Fe_3O_4 NPs nanohybrid's dosage variation (Figure S6); ibuprofen release efficiency with ibuprofen concentration variation in the nanohybrid (Figure S7); and drug release kinetic parameter values (Table S1). (PDF)

■ AUTHOR INFORMATION

Corresponding Author

Himadri Acharya − *Centre for Soft Matters, Department of Chemistry, Assam University, Silchar 788011, India;* orcid.org/0000-0002-8937-9015; Phone: +91 3842 270802; Email: himadriau@yahoo.co.in; Fax: +91 3842 270848

Authors

Anindita Chakraborty − *Centre for Soft Matters, Department of Chemistry, Assam University, Silchar 788011, India;* Present Address: Institute of Chemical Technology, Marathwada Campus, Jalna, Maharashtra 431203, India

Rajat Nandi − *Department of Microbiology, Assam University, Silchar 788011, India*

Diwakar Kumar − *Department of Microbiology, Assam University, Silchar 788011, India;* orcid.org/0000-0002-3050-5179

Complete contact information is available at: https://pubs.acs.org/10.1021/acsomega.3c09135

Notes

The authors declare no competing financial interest.

■ ACKNOWLEDGMENTS

The authors are thankful to the University Grants Commission (UGC), India for the financial assistance.

■ REFERENCES

(1) Sun, Z.; Li, T.; Mei, T.; Liu, Y.; Wu, K.; Le, W.; Hu, Y. Nanoscale MOFs in nanomedicine applications: from drug delivery to therapeutic agents. *J. Mater. Chem. B* **2023**, *11*, 3273−3294.

(2) Ghezzi, M.; Pescina, S.; Padula, C.; Santi, P.; Del Favero, E.; Cantù, L.; Nicoli, S. Polymeric micelles in drug delivery: An insight of the techniques for their characterization and assessment in biorelevant conditions. *J. Controlled Release* **2021**, *332*, 312−336.

(3) Liu, Y.; Bravo, K. M. C.; Liu, J. Targeted liposomal drug delivery: a nanoscience and biophysical perspective. *Nanoscale Horiz.* **2021**, *6*, 78−94.
(4) Zhang, M.; Qin, X.; Zhao, Z.; Du, Q.; Li, Q.; Jiang, Y.; Luan, Y. A self-amplifying nanodrug to manipulate the Janus-faced nature of ferroptosis for tumor therapy. *Nanoscale Horiz.* **2022**, *7*, 198−210.
(5) Amorim, R.; Vilaça, N.; Martinho, O.; Reis, R. M.; Sardo, M.; Rocha, J.; Fonseca, A. M.; Baltazar, F.; Neves, I. C. Zeolite Structures Loading with an Anticancer Compound As Drug Delivery Systems. *J. Phys. Chem. C* **2012**, *116*, 25642−25650.
(6) Manzano, M.; Vallet-Regí, M. Mesoporous Silica Nanoparticles for Drug Delivery. *Adv. Funct. Mater.* **2019**, *30*, No. 1902634.
(7) Kumeria, T. Advances on Porous Nanomaterials for Biomedical Application (Drug Delivery, Sensing, and Tissue Engineering). *ACS Biomater. Sci. Eng.* **2022**, *8*, 4025−4027.
(8) Rivero-Buceta, E.; Encheva, M. E.; Cech, B.; Fernandez, E.; Sastre, G.; Landry, C. C.; Botella, P. Light-activated controlled release of camptothecin by engineering porous materials: the ship in a bottle concept in drug delivery. *Nanoscale* **2023**, *15*, 12506−12517.
(9) Zheng, H.; Zhang, Y.; Liu, L.; Wan, W.; Guo, P.; Nyström, A. M.; Zou, X. One-pot Synthesis of Metal−Organic Frameworks with Encapsulated Target Molecules and Their Applications for Controlled Drug Delivery. *J. Am. Chem. Soc.* **2016**, *138*, 962−968.
(10) Gulati, S.; Choudhury, A.; Mohan, G.; Katiyar, R.; Kurikkal, M. A. M. P.; Kumar, S.; Varma, R. S. Metal−organic frameworks (MOFs) as effectual diagnostic and therapeutic tools for cancer. *J. Mater. Chem. B* **2023**, *11*, 6782−6801.
(11) Yusuf, V. F.; Malek, N. I.; Kailasa, S. K. Review on Metal−Organic Framework Classification, Synthetic Approaches, and Influencing Factors: Applications in Energy, Drug Delivery, and Wastewater Treatment. *ACS Omega* **2022**, *7*, 44507−44531.
(12) Férey, G.; Mellot-Draznieks, C.; Serre, C.; Millange, F.; Dutour, J.; Surblé, S.; Margiolaki, I. A chromium terephthalate-based solid with unusually large pore volumes and surface area. *Science* **2005**, *309*, 2040−2042.
(13) Mokhtari, N.; Dinari, M.; Esmaeiltarkhani, F. K. Imine-Linked Covalent Organic Frameworks: A Biocompatible and pH-Dependent Carrier for In Vitro Sustained Release of Doxorubicin. *ACS Omega* **2023**, *8*, 25565−25573.
(14) Kundu, D.; Banerjee, T. Carboxymethyl Cellulose-Xylan Hydrogel: Synthesis, Characterization, and in Vitro Release of Vitamin B_{12}. *ACS Omega.* **2019**, *4*, 4793−4803.
(15) Tong, P. H.; Zhu, L.; Zang, Y.; Li, J.; He, X. P.; James, T. D. Metal−organic frameworks (MOFs) as host materials for the enhanced delivery of biomacromolecular therapeutics. *Chem. Commun.* **2021**, *57*, 12098−12110.
(16) Zeyni, V.; Karimi, S.; Namazi, H. Surface PEGylation of ZIF-8 metal-organic framework based on magnetic hydroxyapatite as a pH/magnetic targeting responsive system for anticancer drug delivery. *Microporous Mesoporous Mater.* **2023**, *354*, No. 112544.
(17) Chakraborty, A.; Islam, D. A.; Acharya, H. Facile synthesis of CuO nanoparticles deposited zeolitic imidazolate frameworks (ZIF-8) for efficient photocatalytic dye degradation. *J. Solid State Chem.* **2019**, *269*, 566−574.
(18) Velásquez-Hernández, M. d. J.; Ricco, R.; Carraro, F.; Limpoco, F. T.; Linares-Moreau, M.; Leitner, E.; Wiltsche, H.; Rattenberger, J.; Schröttner, H.; Frühwirt, P.; Stadler, E. M.; Gescheidt, G.; Amenitsch, H.; Doonan, C. J.; Falcaro, P. Degradation of ZIF-8 in phosphate buffered saline media. *CrystEngComm* **2019**, *21*, 4538−4544.
(19) Ho, P. H.; Salles, F.; Renzo, F. D.; Trens, P. One-pot synthesis of 5-FU@ZIF-8 and ibuprofen@ZIF-8 nanoparticles. *Inorg. Chim. Acta* **2020**, *500*, No. 119229.
(20) Kumari, S.; Howlett, T. S.; Ehrman, R. N.; Koirala, S.; Trashi, O.; Trashi, I.; Wijesundara, Y. H.; Gassensmith, J. J. In vivo biocompatibility of ZIF-8 for slow release via intranasal administration. *Chem. Sci.* **2023**, *14*, 5774−5782.
(21) Abdelhamid, H. N.; Kassem, D. H.; Hathout, R. M. Magnetic Nanoparticles Encapsulated Zeolitic Imidazolate Frameworks: A New Delivery System for Crocin. *J. Cluster Sci.* **2023**, 1−7, DOI: 10.1007/s10876-023-02526-4.
(22) Abdelhamid, H. N. Zeolitic Imidazolate Frameworks (ZIF-8) for Biomedical Applications: A Review. *Curr. Med. Chem.* **2021**, *28*, 7023−7075.
(23) Abdelhamid, H. N. An introductory review on advanced multifunctional materials. *Heliyon* **2023**, *9*, No. e18060.
(24) Lawson, H. D.; Walton, S. P.; Chan, C. Metal-Organic Frameworks for Drug Delivery: A Design Perspective. *ACS Appl. Mater. Interfaces* **2021**, *13*, 7004−7020.
(25) Kolosnjaj-Tabi, J.; Javed, Y.; Lartigue, L.; Volatron, J.; Elgrabli, D.; Marangon, I.; Giammarino, P.; Caron, B.; Figuerola, A.; Luciani, N.; Pellegrino, T.; Alloyeau, D.; Gazeau, F. The One Year Fate of Iron Oxide Coated Gold Nanoparticles in Mice. *ACS Nano* **2015**, *9*, 7925−7939.
(26) Cabral, H.; Miyata, K.; Osada, K.; Kataoka, K. Block Copolymer Micelles in Nanomedicine Applications. *Chem. Rev.* **2018**, *118*, 6844−6892.
(27) Khan, M. I.; Hossain, M. I.; Hossain, M. K.; Rubel, M. H. K.; Hossain, K. M.; Mahfuz, A. M. U. B.; Anik, M. I. Recent Progress in Nanostructured Smart Drug Delivery Systems for Cancer Therapy: A Review. *ACS Appl. Bio Mater.* **2022**, *5*, 971−1012.
(28) Fu, P. P.; Xia, Q.; Hwang, H. M.; Ray, P. C.; Yu, H. Mechanisms of nanotoxicity: Generation of reactive oxygen species. *J. Food Drug Anal.* **2014**, *22*, 64−75.
(29) Zhan, S.; Wang, J.; Wang, W.; Cui, L.; Zhao, Q. Preparation and in vitro release kinetics of nitrendipine-loaded PLLA−PEG−PLLA microparticles by supercritical solution impregnation process. *RSC Adv.* **2019**, *9*, 16167−16175.
(30) Kurečič, M.; Mohan, T.; Virant, N.; Maver, U.; Stergar, J.; Gradišnik, L.; Kleinschek, K. S.; Hribernik, S. A green approach to obtain stable and hydrophilic cellulose-based electrospun nanofibrous substrates for sustained release of therapeutic molecules. *RSC Adv.* **2019**, *9*, 21288−21301.
(31) van Meerloo, J.; Kaspers, G. J. L.; Cloos, J. Cell Sensitivity Assays: The MTT Assay. *Methods Mol. Biol.* **2011**, *731*, 237−245.
(32) Alqadami, A. A.; Naushad, M.; Alothman, Z. A.; Ghfar, A. A. Novel Metal−Organic Framework (MOF) Based Composite Material for the Sequestration of U(VI) and Th(IV) Metal Ions from Aqueous Environment. *ACS Appl. Mater. Interfaces* **2017**, *9* (41), 36026−36037.
(33) Singh, K. K.; Senapati, K. K.; Sarma, K. C. Synthesis of superparamagnetic Fe_3O_4 nanoparticles coated with green tea polyphenols and their use for removal of dye pollutant from aqueous solution. *J. Environ. Chem. Eng.* **2017**, *5*, 2214−2221.
(34) Chakraborty, A.; Acharya, H. Magnetically separable Fe_3O_4 NPs/MIL-53(Al) nanocomposite catalyst for intrinsic OPD oxidation and colorimetric hydrogen peroxide detection. *Colloids Surf., A* **2021**, *624*, No. 126830.
(35) Kaur, H.; Mohanta, G. C.; Gupta, V.; Kukkar, D.; Tyagi, S. Synthesis and characterization of ZIF-8 nanoparticles for controlled release of 6-mercaptopurine drug. *J. Drug Delivery Sci. Technol.* **2017**, *41*, 106−112.
(36) Verma, V. K.; Subbiah, S. Prospects of Silk Sericin as an Adsorbent for Removal of Ibuprofen from Aqueous Solution. *Ind. Eng. Chem. Res.* **2017**, *56*, 10142−10154.
(37) Yao, H.; Ishikawa, Y. Finite Size Effect on Magneto-Optical Responses of Chemically Modified Fe_3O_4 Nanoparticles Studied by MCD Spectroscopy. *J. Phys. Chem. C* **2015**, *119*, 13224−13230.
(38) Tang, J.; Myers, M.; Bosnick, K. A.; Brus, L. E. Magnetite Fe_3O_4 Nanocrystals: Spectroscopic Observation of Aqueous Oxidation Kinetics. *J. Phys. Chem. B* **2003**, *107*, 7501−7506.
(39) El-Trass, A.; ElShamy, H.; Mehasseb, I. E.; Kemary, M. E. CuO nanoparticles: Synthesis, characterization, optical properties and interaction with amino acids. *Appl. Surf. Sci.* **2012**, *258*, 2997−3001.
(40) Guo, X.; Wu, J.; Yiu, Y.-M.; Hu, Y.; Zhu, Y.-J.; Sham, T.-K. Drug-nanocarrier interaction-tracking the local structure of calcium silicate upon ibuprofen loading with X-ray absorption near edge structure (XANES). *Phys. Chem. Chem. Phys.* **2013**, *15*, 15033−15040.

https://doi.org/10.1021/acsomega.3c09135
ACS Omega 2024, 9, 32418−32428

(41) Shen, L.-H.; Bao, J.-F.; Wang, D.; Wang, Y.-X.; Chen, Z.-W.; Ren, L.; Zhou, X.; Ke, X.-B.; Chen, M.; Yang, A.-Q. One-step synthesis of monodisperse, water-soluble ultra-small Fe_3O_4 nanoparticles for potential bio-application. *Nanoscale* **2013**, *5*, 2133−2141.
(42) Lestari, W. W.; Arvinawati, M.; Martien, R.; Kusumaningsih, T. Green and facile synthesis of MOF and nano MOF containing zinc(II) and benzen 1,3,5-tri carboxylate and its study in ibuprofen slow-release. *Mater. Chem. Phys.* **2018**, *204*, 141−146.
(43) Xie, Y.; Liu, X.; Ma, X.; Duan, Y.; Yao, Y.; Cai, Q. Small Titanium-Based MOFs Prepared with the Introduction of Tetraethyl Orthosilicate and Their Potential for Use in Drug Delivery. *ACS Appl. Mater. Interfaces* **2018**, *10*, 13325−13332.
(44) Horcajada, P.; Serre, C.; Regí, M. V.; Sebban, M.; Taulelle, F.; Férey, G. Metal−Organic Frameworks as Efficient Materials for Drug Delivery. *Angew. Chem., Int. Ed.* **2006**, *45*, 5974−5978.
(45) Motakef-Kazemi, N.; Shojaosadati, S. A.; Morsali, A. In situ synthesis of a drug-loaded MOF at room temperature. *Microporous Mesoporous Mater.* **2014**, *186*, 73−79.
(46) Ulbrich, K.; Holá, K.; Šubr, V.; Bakandritsos, A.; Tuček, J.; ZboŘI, R. Targeted Drug Delivery with Polymers and Magnetic Nanoparticles: Covalent and Noncovalent Approaches, Release Control, and Clinical Studies. *Chem. Rev.* **2016**, *116*, 5338−5431.
(47) Rovers, S. A.; Hoogenboom, R.; Kemmere, M. F.; Keurentjes, J. T. F. Repetitive on-demand drug release by magnetic heating of iron oxide containing polymeric implants. *Soft Matter* **2012**, *8*, 1623−1627.
(48) Ramos, V. C.; Reyes, C. B. G.; García, G. M.; Quesada, M. I. S.; Barrero, F. J. M. C.; Rábago, J. J. S.; Polo, M. S. ZIF-8 and Its Magnetic Functionalization as Vehicle for the Transport and Release of Ciprofloxacin. *Pharmaceutics* **2022**, *14*, 2546.
(49) Nabipour, H.; Sadra, M. H.; Bardajee, G. R. Synthesis and characterization of nanoscale zeolitic imidazolate frameworks with ciprofloxacin and their applications as antimicrobial agents. *New J. Chem.* **2017**, *41*, 7364−7370.
(50) Karimi Alavijeh, R.; Akhbari, K. Biocompatible MIL-101(Fe) as a Smart Carrier with High Loading Potential and Sustained Release of Curcumin. *Inorg. Chem.* **2020**, *59*, 3570−3578.

https://doi.org/10.1021/acsomega.3c09135
ACS Omega 2024, 9, 32418−32428